Q. J. R. Meteorol. Soc. 1994), **120,** pp. 1255–1265 551.515.21

The development of potential vorticity in a hurricane-like vortex

By J. D. MÖLLER and R. K. SMITH*
University of Munich, Germany

(Received 23 August 1993; revised 15 December 1993)

SUMMARY

We investigate the time evolution of the potential-vorticity distribution in an axisymmetric hurricane-like vortex using a numerical model based on a formulation by Schubert and Alworth. In particular, we compare the vortex response to an annular heating function with that in the analytic calculation by Schubert and Alworth in which the maximum heating rate occurs on the vortex axis. The annular heating function is intended to better represent the latent-heat release in the eye-wall clouds of a hurricane. We show that after about four days of integration time in the Schubert–Alworth calculation, the isentropes near the vortex centre, and hence the prescribed heating function, become concentrated near the surface in physical space. In comparison, for the annular heating distribution the descent of the isentropes is less marked and the vertical distribution of the heating in physical space remains more realistic *vis-à-vis* a hurricane. It is significant that in this case the potential-vorticity maximum lies not on the vortex axis, as in the Schubert–Alworth calculation, but close to the radius of maximum heating. This appears to be consistent with observations in hurricanes. Finally we show that, counter to intuition, there is greater subsidence on the vortex axis in the case where the heating is a maximum on the axis. A dynamical explanation is offered for this result.

1. INTRODUCTION

Much of our understanding of the dynamics of tropical-cyclone motion is based on results from barotropic vortex models in which the asymmetry of the relative-vorticity distribution has been shown to play an important role. The asymmetry can be inverted to obtain the asymmetry in the stream function and from this the velocity of flow across the vortex centre can be determined; this velocity is a close approximation to the translation velocity of the vortex (Smith *et al.* 1990). A natural extension of the ideas to baroclinic vortices would point to the importance of the asymmetry in the potential-vorticity (PV) distribution. If the vortex is in some sense in balance (e.g. if hydrostatic and cyclostrophic balance pertain), the PV asymmetry can be inverted also to obtain the flow across the vortex axis. As a preliminary to such an extension to tropical cyclones, a better understanding of the PV evolution and its mature distribution in these vortices is required, even in symmetric models of these disturbances. A first step in this direction was made by Schubert and Alworth (1987, henceforth referred to as SA) who studied the PV evolution in a symmetric hurricane-like vortex in which latent heat release was represented by a prescribed heating function in a cylindrical region on an f-plane. The formulation was based on Eliassen's balanced vortex model (Eliassen 1952) expressed in isentropic (Θ) and potential radius (R) coordinates and leads to a prediction equation for the potential density (inverse PV) and a diagnostic equation for a function, M^*, which is related to the Montgomery potential. Knowledge of the distribution of Montgomery potential at a particular time enables flow variables such as the tangential velocity and the pressure to be determined. By choosing a simple heating distribution and ignoring the effects of friction, SA were able to obtain an analytic solution to the potential density equation. From this they calculated the evolution of the PV field as a function of time in R–Θ space.

In this paper we re-examine the SA solution and show that, as the vortex develops, the specified heating distribution becomes progressively more unrealistic *vis-à-vis* a tropical cyclone. The reason is that, near the vortex axis, there is a very marked descent

* Corresponding author: Meteorological Institute, University of Munich, Theresienstr. 37, 80333 Munich, Germany.

of the isentropes, whereupon, in physical space, the heating function becomes more and more concentrated in a disk-like region at low levels. Here, we present numerical integrations of the SA equations and show that a more realistic hurricane-like vortex is obtained by prescribing the heating in an annular region. This has implications for the PV structure in the 'eye' region of the model vortex and for the strength of the subsiding motion in the eye as described in section 3. In the following section we describe briefly the model formulation and method of solution.

2. The balanced model

(a) *Model equations*

The reader is referred to SA for details of the model formulation in (R, Θ) coordinates. The key equations are the equation for the potential pseudodensity, σ^*, and a function, M^*, related to the Montgomery potential, M, by the formula $M^* = M + v^2/2$, where v is the tangential velocity. These equations have the form

$$\frac{\partial \sigma^*}{\partial T} + \frac{1}{R}\frac{\partial}{\partial R}(R\dot{R}\sigma^*) + \frac{\partial}{\partial \Theta}(\dot{\theta}\sigma^*) = 0 \tag{1}$$

and

$$\left\{f^2 - R^3\frac{\partial}{\partial R}\left(\frac{1}{R^3}\frac{\partial M^*}{\partial R}\right)\right\}\frac{\partial^2 M^*}{\partial \Theta^2} + \left(\frac{\partial^2 M^*}{\partial R \partial \Theta}\right)^2 + \Gamma\sigma^*\left(f + \frac{2}{f}\frac{\partial M^*}{\partial R}\right)^2 = 0 \tag{2}$$

where $\dot{R}$ is the friction, $\dot{\theta}$ is the heating function, f is the Coriolis parameter, T is the time, $\Gamma(p) = (\mathrm{R_L}/p_0)(p/p_0)^{\kappa-1}$, $\kappa = R_\mathrm{L}/c_p$, c_p denotes the specific heat at constant pressure, $p_0 = 1000$ mb and R_L the specific gas constant. The potential radius, R, is defined as the radius at which an air parcel would attain zero tangential velocity if displaced radially while conserving angular momentum and is related to the physical radius, r, by the formula $fR^2 = fr^2 + 2vr$. Use of the potential radius coordinate not only facilitates a compact form of the equations, but also provides a better resolution than physical radius in regions of strong radial gradient of potential vorticity. The conventional Ertel potential vorticity, P, is related to σ^* through the formula $P = (f\sigma_0)/\sigma^*$, where σ_0 $(=(p_0 - p_\mathrm{T})/(\Theta_\mathrm{T} - \Theta_\mathrm{B}))$ is a constant reference density, where $p_\mathrm{T} = 100$ mb, $\Theta_\mathrm{B} = 300$ K, $\Theta_\mathrm{T} = 360$ K and subscripts B and T are bottom and top. Our approach differs from that of SA in that Eq. (1) is integrated numerically in time, whereas SA obtained an analytical solution for σ^* for a specific analytically prescribed heating function. If the motion is frictionless, as is assumed here, R is materially conserved whereupon $\dot{R} = 0$. In this case the second term in Eq. (1) vanishes. The third term in this equation involves the diabatic heating rate, θ, which in our calculation is prescribed by the formula

$$\dot{\theta} = 2Q_0(R/R_0)\exp\{-(R/R_0)^2\}\sin Z \tag{3}$$

where $Q_0 = 27$ K day^{-1}, $R_0 = 250$ km and $Z = \pi(\Theta - \Theta_\mathrm{B})/(\Theta_\mathrm{T} - \Theta_\mathrm{B})$.

(b) *Boundary conditions*

The calculations are carried out in a cylindrical domain in (R, Θ) space, the top at $\Theta = \Theta_\mathrm{T}$, the bottom at $\Theta = \Theta_\mathrm{B}$, and the lateral boundary at $R = R_\mathrm{B}$. The same boundary conditions are used as in SA. The boundary conditions on M^* express the facts that: the upper boundary is an isobaric surface with Exner function Π_T; the lower boundary has

zero geopotential; the axis is a line of symmetry and the disturbance magnitude is negligible at the lateral boundary. These conditions take the form

$$\frac{\partial M^*}{\partial \Theta} = \Pi_T \text{ at } \Theta = \Theta_T \tag{4}$$

$$\left(f^2 + \frac{2}{R}\frac{\partial M^*}{\partial R}\right)\left(\Theta\frac{\partial M^*}{\partial \Theta} - M^*\right) + \frac{1}{2}\left(\frac{\partial M^*}{\partial R}\right)^2 = 0 \text{ at } \Theta = \Theta_B \tag{5}$$

$$\frac{\partial M^*}{\partial R} = 0 \text{ at } R = 0 \tag{6}$$

$$M^* = c_p\Theta_B + \frac{c_p p_0}{\sigma_0(1+\kappa)}\left\{1 - \left(\frac{\bar{p}}{p_0}\right)^{1+\kappa}\right\} \text{ at } R = R_B \tag{7}$$

where $\bar{p} = p_T + \sigma_0(\Theta_T - \Theta)$ denotes the basic state pressure.

(c) *Numerical method*

The prognostic equation for $\sigma^*(=f\sigma_0/P)$ is solved by a predictor–corrector method similar to that used by Hsu and Arakawa (1990) with the initial condition $\sigma^* = \sigma_0$ (note that initially $P = f$). This time integration scheme is positive definite and ensures that the pseudodensity is positive for all time. In the method, the term $\partial(\dot{\theta}\sigma^*)/\partial\Theta$ in Eq. (1), is evaluated using a predictor–corrector method. First the predictor is computed and then the corrector for the interior field. The lateral boundaries at $R = 0$ and R_B are included in the interior sweep. SA specified the boundary values for σ^* in Eq. (1) at $\Theta = \Theta_T$ and Θ_B from the analytic solution using l'Hospital's rule. Here, the boundary values are determined by a Taylor series approximation with a second-order space differencing as follows

$$\sigma_{i,j\max} = 2\sigma_{i,j\max-1} - \sigma_{i,j\max-2}, \quad \text{at } \Theta = \Theta_T \tag{8}$$

$$\sigma_{i,0} = 2\sigma_{i,j-1} - \sigma_{i,j-2}, \quad \text{at } \Theta = \Theta_B \tag{9}$$

where the index, i, denotes the horizontal grid points and j the vertical grid points.

Since the pseudodensity is always positive, the nonlinear diagnostic Eq. (2) remains elliptic and can be solved uniquely for the Montgomery potential, M^*, to recover the wind and mass fields. In actual fact, Eq. (2) was first expressed in terms of $M'(R, \Theta)$, the deviation of $M^*(R, \Theta)$ from its basic state value $\bar{M}(\Theta)$. The resulting equation was then solved by an iterative successive over-relaxation (SOR) method at every time-step. An over-relaxation parameter $\beta = 1.7$ was found to be optimal and enabled the number of iterations to be reduced to 800–1200, compared with SA who found that 'several thousand' iterations were necessary when using a relaxation method 'in the spirit of Gauss-Seidel' to obtain convergence. As a first guess, M' was taken to be zero at the first time-step. At subsequent time-steps the value at the previous time-step was used.

3. Results and discussion

As a check on the accuracy of the numerical model, Eqs. (1) and (2) were integrated for the heating function specified by SA, shown in Fig. 1(a). Initially the maximum heating rate of 30 K day^{-1} lies on the axis of the domain at the mid-Θ level (330 K), corresponding with a height of about 6 km. Good agreement was found between the tangential wind speed and PV distributions calculated by SA and the corresponding ones

obtained from the numerical calculation. For later comparison, Fig. 1(b) shows the tangential-velocity distribution, $v\ (R, \Theta)$, after 120 hours. At this time, the maximum speed is 48 m s^{-1} which exceeds hurricane strength (33 m s^{-1}), the latter being achieved after 96 hours of integration.

It is of interest to examine the behaviour of the isentropes themselves as the vortex evolves. Figure 1(c) shows their structure at 120 hours in (R, z) space where z is physical height. The latter was determined from the formula

$$z = \left(M^* - \frac{v^2}{2} - \Theta\Pi\right)/g \tag{10}$$

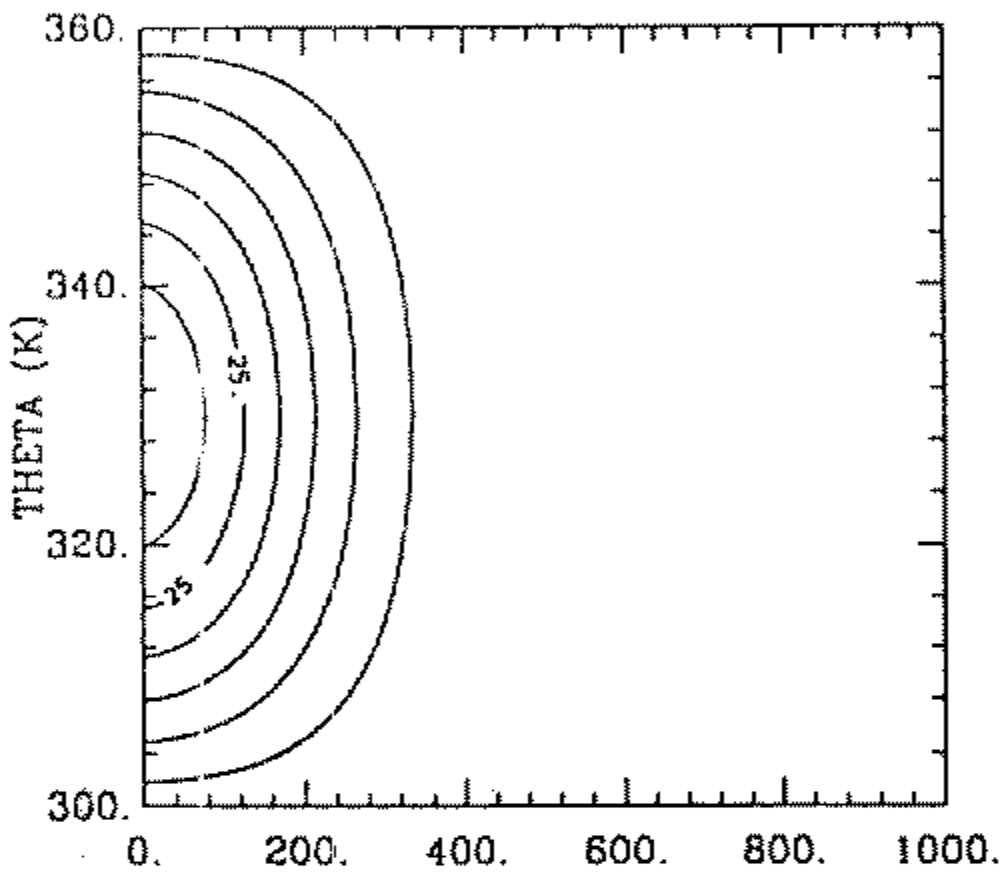

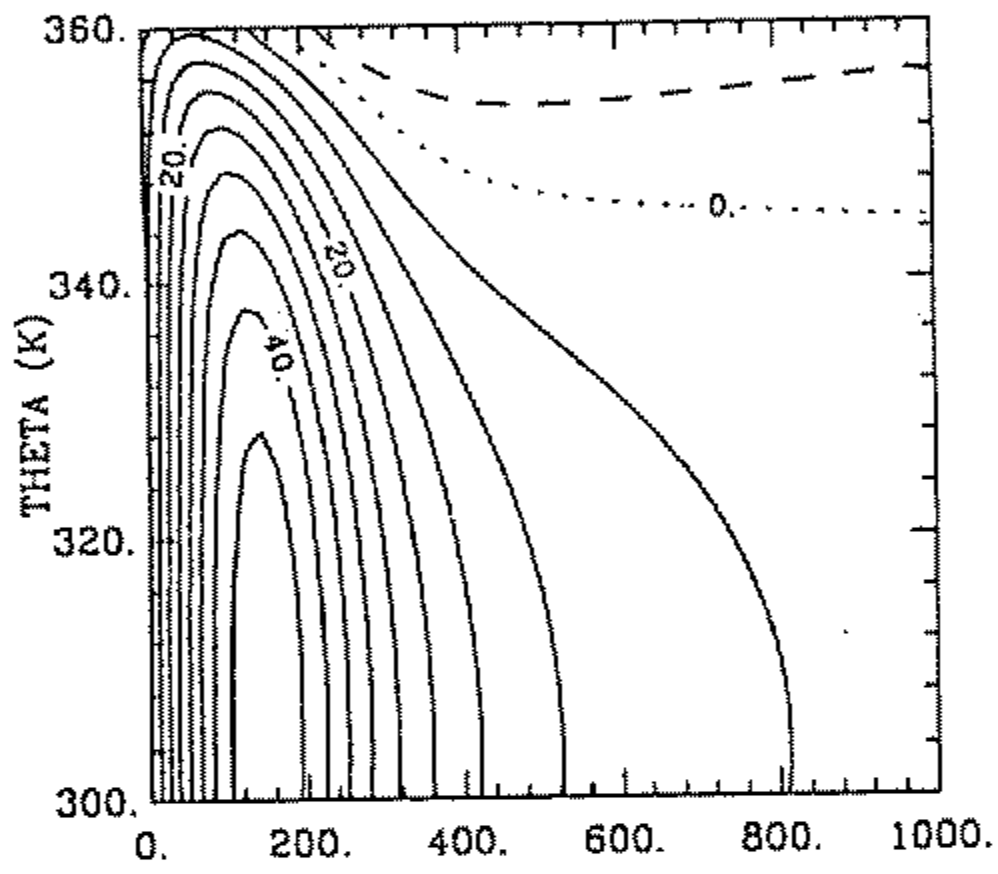

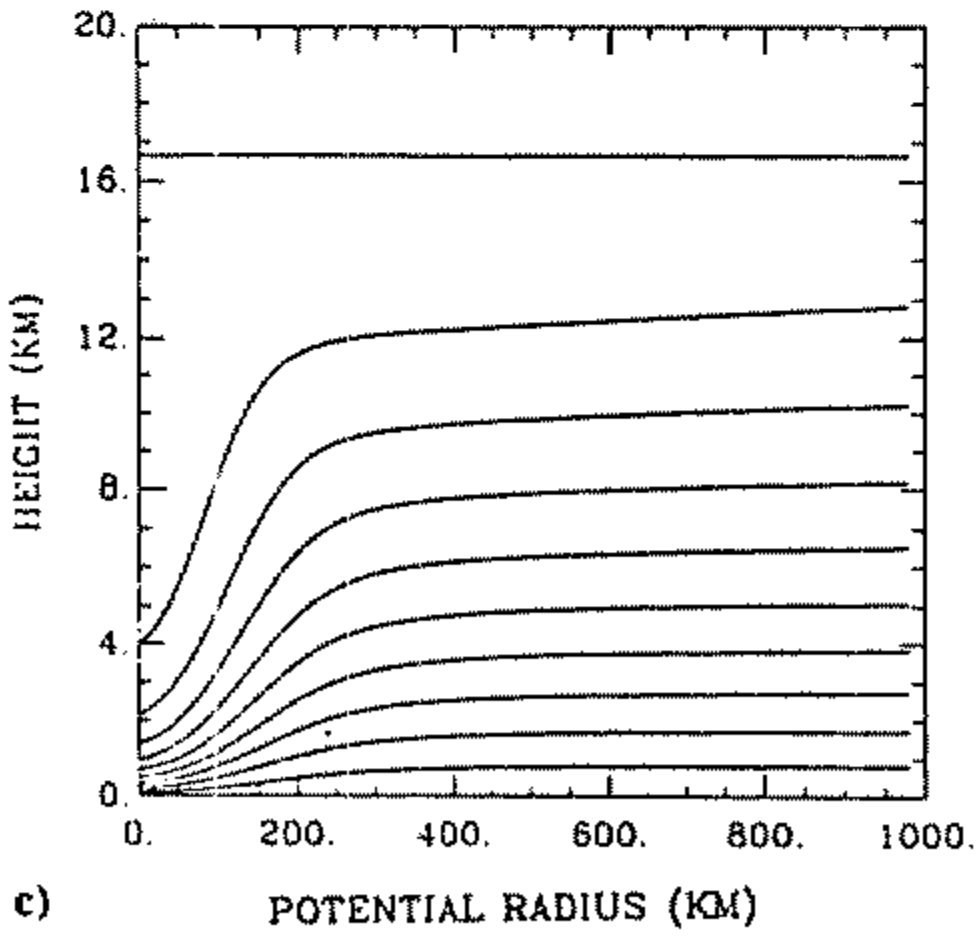

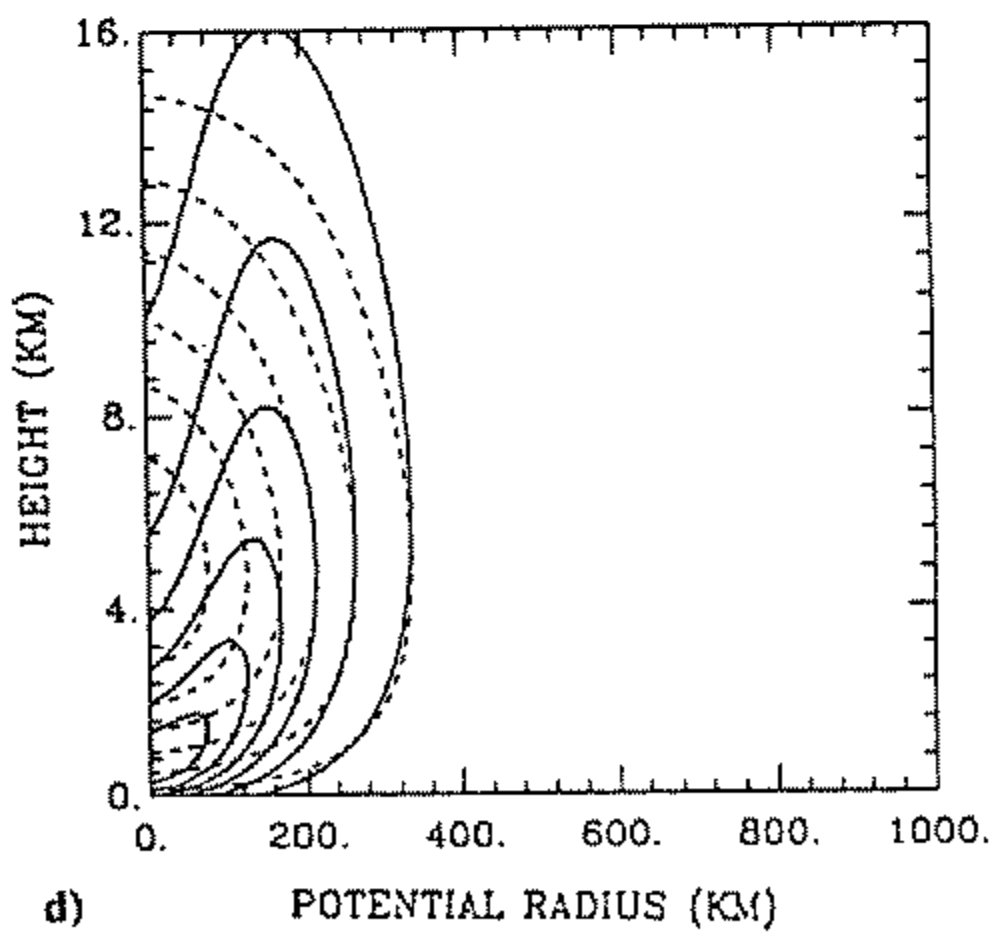

Figure 1. Calculation with Schubert and Alworth's heating function. (a) Isolines of the heating rate as a function of potential temperature, Θ, and potential radius, R. The maximum heating rate of 30 K day^{-1} occurs on the axis, $R = 0$. Contour interval is 4.5 K day^{-1}. (b) Isotachs of the tangential wind, $v\ (R, \Theta)$, at 120 hours. Contour interval is 5 m s^{-1}. (c) Isentropic surfaces in (R, z) space. Contour interval is 6 K from 300 K to 360 K. (d) Isolines of the heating rate in (R, z) space at 120 hours compared with those at the initial time (dashed line). Contour interval as in (a).

where g denotes the acceleration due to gravity and $M^* = \overline{M}^* + M'^*$. The isentrope distribution at large potential radius in this figure is essentially that of the initial distribution. It is clear that after five days there has been a marked descent of the isentropes along the vortex axis. Thus the heating distribution, which is specified as a function of Θ, becomes progressively more concentrated at lower and lower levels. This is illustrated in Fig. 1(d) which compares the heating function in (R, z) space at 120 hours with the initial distribution (dashed line). The descent of the heating function is not at all realistic in relation to a mature hurricane. Indeed, in the latter case, as soon as the eye has formed, one would expect the maximum diabatic heating rate to lie off the axis in the region of the eye-wall clouds.

Unrealistic descent of the isentropes cannot be avoided with a fixed heating function. However, the concentration of the descent on the axis could be reduced by specifying a more representative fixed heating function. We have investigated a variety of alternative heating functions and present here the results of an integration with the one shown in Fig. 2(a). This has a maximum amplitude of 27 K day^{-1} and lies at a potential radius of about 160 km. Figure 2(b) shows the tangential velocity distribution in this calculation, again at 120 hours. The maximum of 52 m s^{-1} is comparable in strength with that in the SA calculation at this time, but occurs at a potential radius of about 300 km, compared with 160 km in the SA case. The relationship between potential radius and geometric radius, r, at 120 hours is illustrated by the contours of r (R, Θ) shown in Fig. 2(e). Near the surface the iso-line of 100 km physical radius corresponds with a potential radius of 400 km at this time, but near the top boundary the potential radius is only about 40 km. Typically, as the vortex evolves, the potential radius of a given physical radius increases with time where the tangential velocity increases with time and it decreases where the tangential velocity decreases.

The isentropes and heating function in (R, z) space at 120 hours are shown in Figs. 2(c) and 2(d), respectively. As in the SA calculation, the isentropes and hence the region of maximum heating descend, but the amount of descent is much less extreme. Thereupon, both the heating distribution and the pattern of isentropes are more realistic *vis-à-vis* that of a mature hurricane, at least in the later stages of the calculation. At early times, of course, the specification of an annular heating distribution is not realistic in relation to the hurricane precursor.

Figure 3 compares the PV evolution corresponding with the two foregoing numerical integrations as exemplified by the fields at 48 and 120 hours. Shown are the distributions at 120 hours in both (R, Θ) and (R, z) cross-sections. In both model integrations the broad-scale evolution is similar, with a strong cyclonic PV anomaly developing along the axis and a broader anticyclonic anomaly aloft. One can interpret the evolution in two ways. Haynes and McIntye (1987, 1990) showed that if P is regarded as the mixing ratio of a hypothetical 'PV substance' in analogy with that of a chemical tracer, then the amount of this substance $\int_V \rho P \, dV$, contained between two isentropic surfaces cannot change, even in the presence of diabatic and frictional processes. Here ρ is the fluid density and V the volume between the two surfaces. Nevertheless, in the presence of diabatic sources and sinks, the mass $\int_V \rho \, dV$ between the two isentropes changes so that the 'mixing-ratio' P, itself, changes to preserve $\int_V \rho P \, dV$. For example, in the present case, diabatic heating in a region of stable-stratified fluid leads to a lowering of the isentropes in that region (compare Figs. 1(c) and 2(c)). This leads to a reduction of mass between any two isentropic surfaces below the heating maximum, with a consequent increase in P. Above the heating maximum, the mass between two isentropic surfaces is increased and P is decreased. In effect, the heating gives rise to a dipole anomaly of P with the cyclonic anomaly in the lower atmosphere and the anticyclonic anomaly aloft,

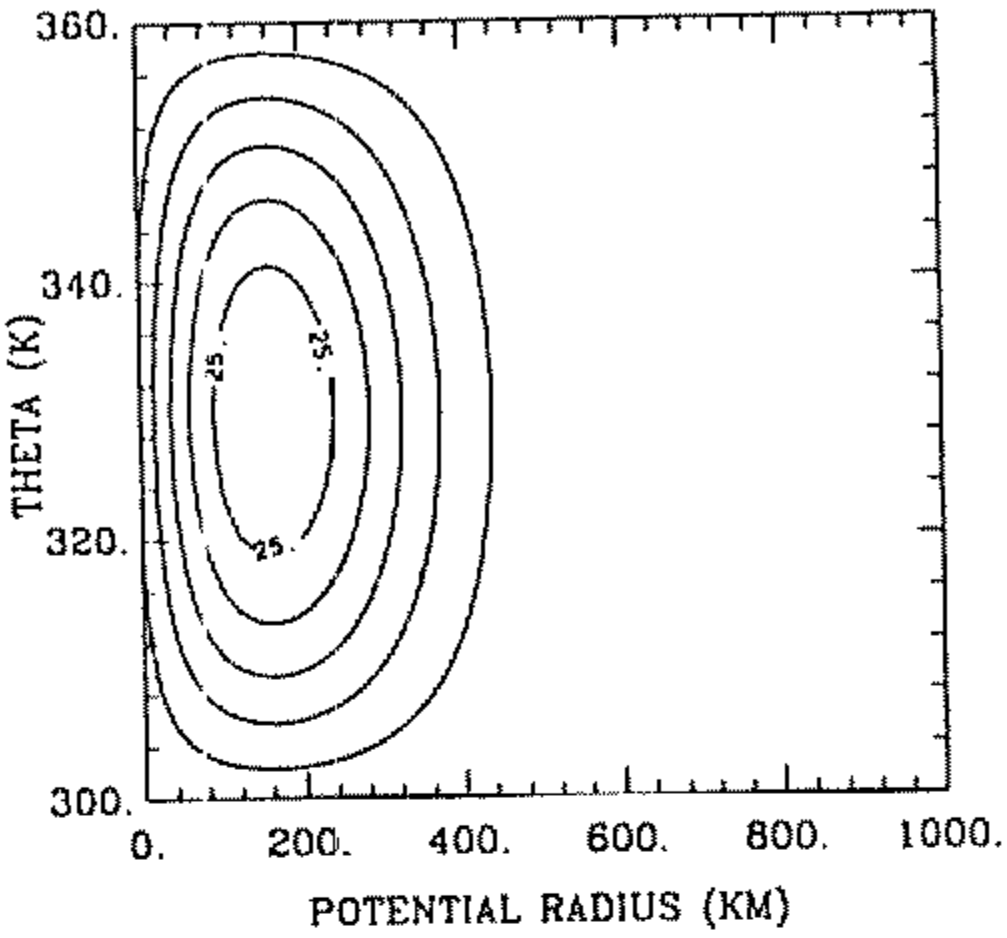

a)

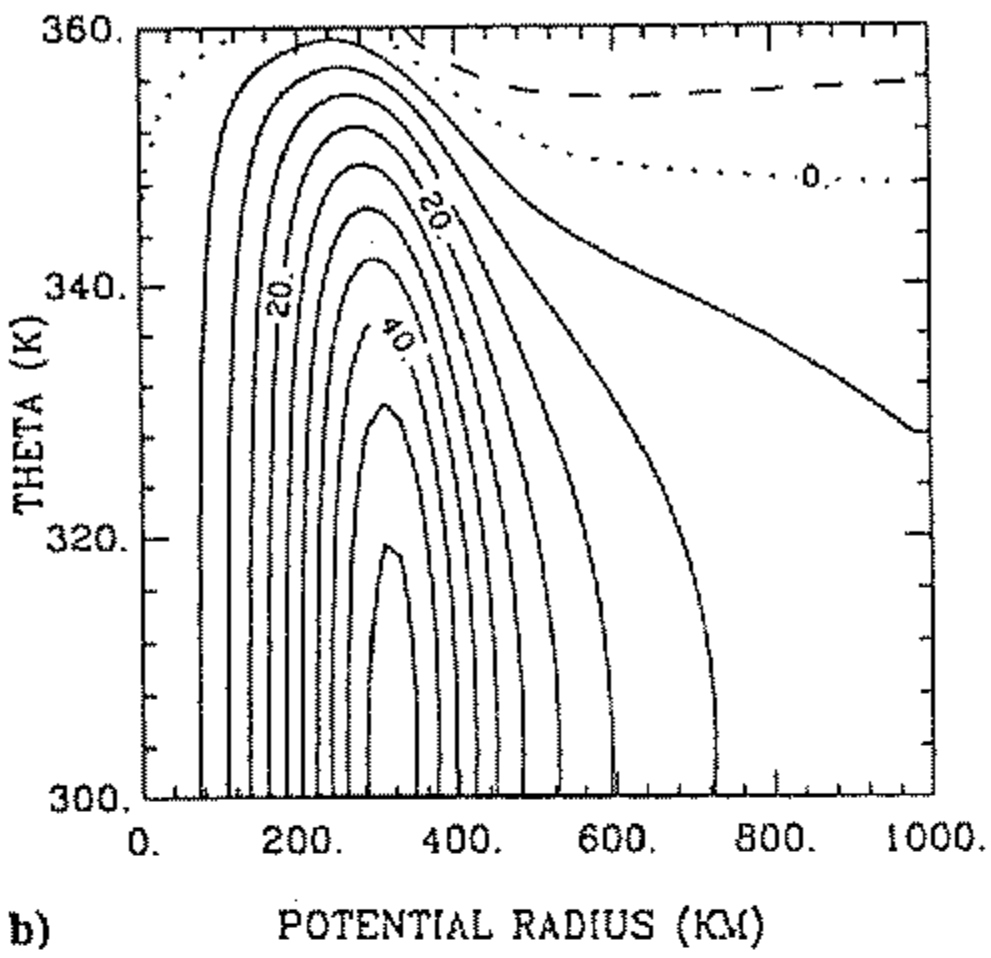

b)

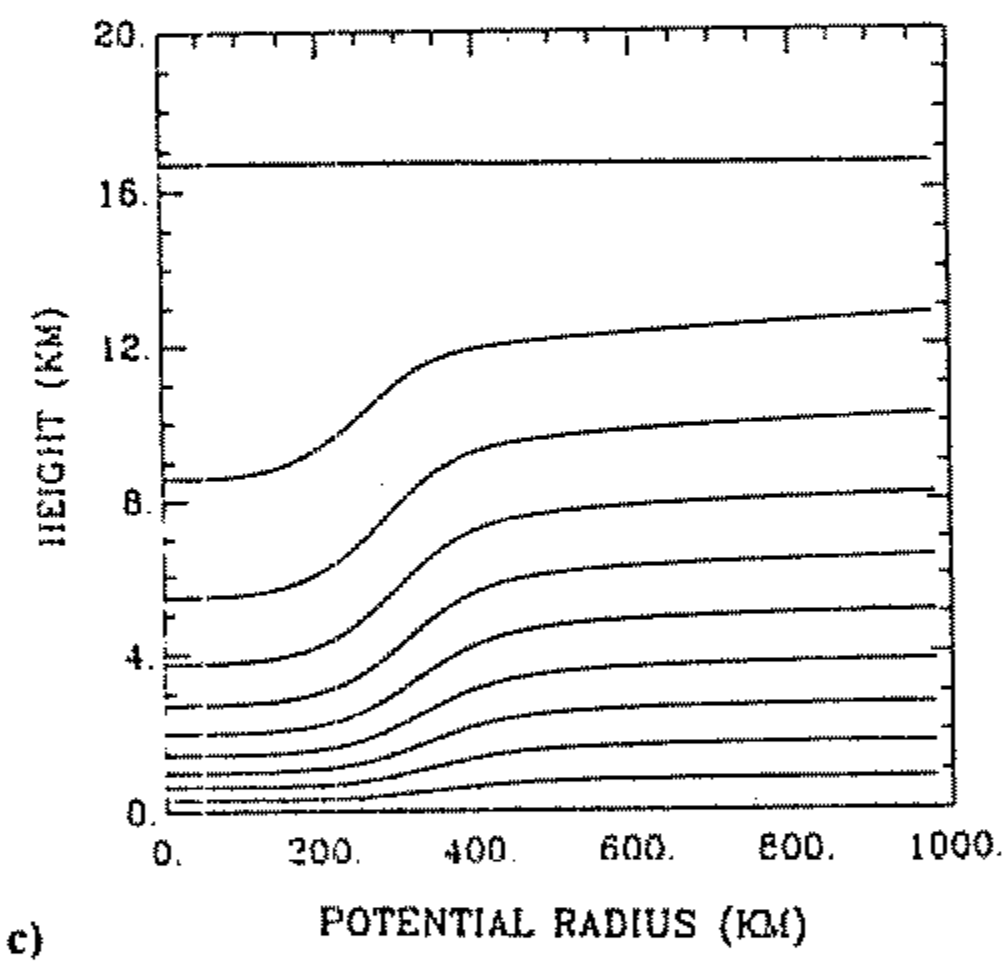

c)

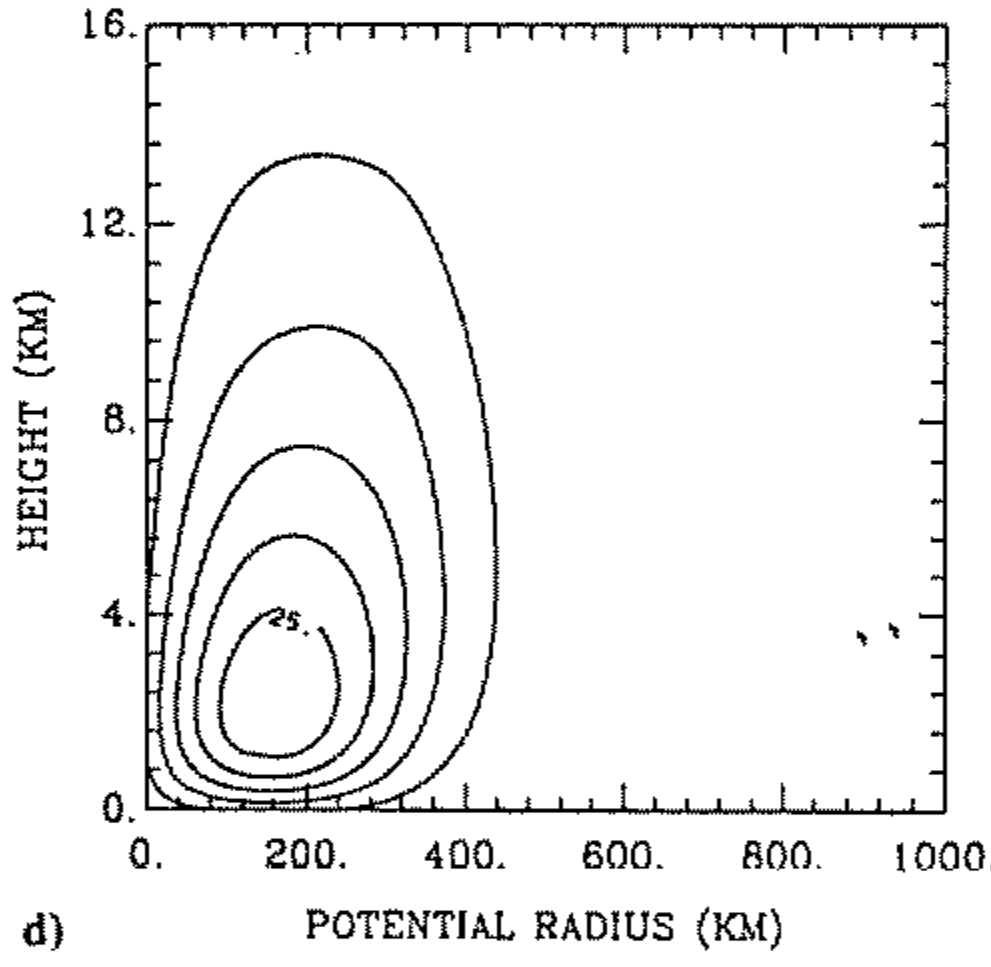

d)

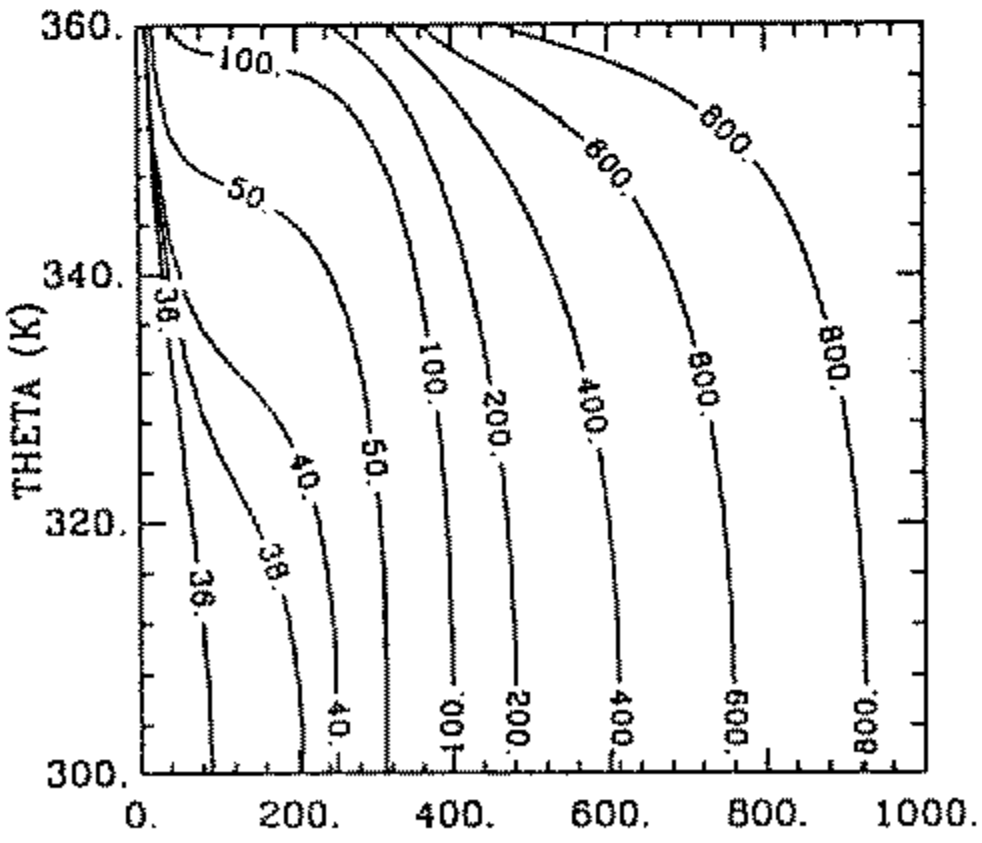

e)

Figure 2. Similar to Fig. 1, but for the annular heating function defined in section 2 (a). The maximum heating rate is 27 K day^{-1} and occurs at $R = 200$ km. (e) Isolines of the physical radius, r in (R, Θ) space (km) at 120 hours.

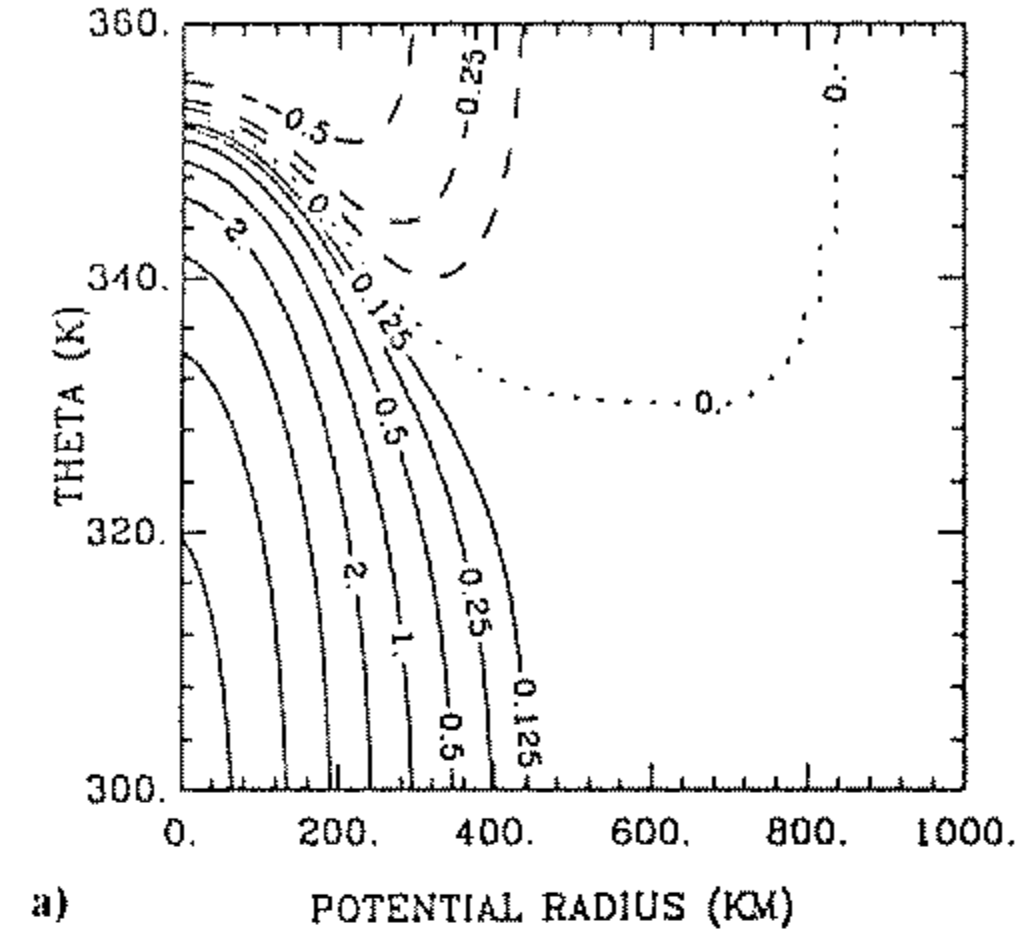

Figure 3. Isolines of dimensionless potential vorticity anomaly (P/f) in (R, Θ) space for the heating function in Fig. 1(a) at (a) 48 hours and (b) 120 hours, and for the heating function in Fig. 2(a) at (c) 48 hours and (d) 120 hours. (e) and (f) show, respectively, the fields in (b) and (d) plotted in (R, z) space.

as exemplified in all panels of Fig. 3. To better understand the vertical asymmetry of this dipole and to interpret the PV distribution in (R, z) space, it is helpful to consider the conservation equation for P itself. In the presence of diabatic forcing and absence of friction, this may be written in vector form as

$$\frac{\partial P}{\partial t} + \mathbf{u} \cdot \nabla P = \frac{1}{\rho} \boldsymbol{\zeta}_a \cdot \nabla \dot{\theta} \tag{11}$$

where $\boldsymbol{\zeta}_a$ is the absolute vorticity vector and other quantities have been defined. According to this equation, diabatic heating leads to the creation of P at a rate proportional to $\boldsymbol{\zeta}_a \cdot \nabla\theta$, which at early times in the present problem is approximately equal to $f\,\partial\dot{\theta}/\partial z$. Again, it follows that the rate is positive below the heating maximum and negative above it, leading to a vertically oriented dipole anomaly. However, as the heating-induced secondary circulation develops, the PV is advected with it (second term on the left of Eq. (11)). Accordingly, the positive PV anomaly generated below the heating maximum is carried to high levels within the annulus of heating, while the negative anomaly is carried by the upper-level outflow to large radii where it experiences subsidence in the return branch of the circulation. These structures are clearly evident in Fig. 3. Note that, as the vortex evolves, the absolute vorticity field progressively deviates from the planetary vorticity and the diabatic source term becomes distorted as well.

There are clear differences in detail between the PV fields in SA calculation and our own, especially in the inner region. In the former, the maximum cyclonic PV anomaly occurs on the vortex axis along which the heating is a maximum and in the later stages of the evolution, the negative anomaly is confined to outer radii (compare Figs. 3(a) and (b)). In particular, the maximum relative vorticity occurs at the vortex axis. In contrast, when the heating is confined to an annular region round the vortex, the maximum PV is located within this annulus, and air with low PV is able to penetrate into the vortex core from aloft in the model vortex's eye region (Figs. 3(c) and (d)). Figures 3(e) and (f) show the PV anomaly in (R, z) space after 120 hours for both cases. When viewing Fig. 3 one should keep in mind the distortion implied by the potential radius coordinate (see, for example, Fig. 2(e)). In particular, the PV maximum near the surface in Figs. 3(d) and (f) occurs at a physical radius of about 35 km and corresponds with a maximum relative vorticity at or near this radius. Again, this would appear to be in line with observations which indicate that the vorticity is maximized near the radius of maximum wind (RMW) and not at the centre as is often assumed. Gray and Shea (1973, Fig. 15) showed in their analyses of composite data from 533 radial flights that the vorticity is a maximum at about 5 km inside the RMW. A recent analysis of data for hurricane *Gloria* (1985) by Shapiro and Franklin (private communication) shows a similar feature. This analysis, based on data at the 450 mb level which is highly filtered in the azimuthal direction, shows the maximum of relative vorticity in a ring about 7–8 km inside the RMW.

It is of interest to examine the reason for the greater descent of the isentropes in the SA calculation compared with the present one. First, one must bear in mind that the descent is associated with both diabatic and adiabatic processes. Based on the initial magnitude and vertical distribution of the heating functions, which are the same in both calculations, one would expect the same amount of descent to be associated with the diabatic contribution, at least at the radius of maximum heating and despite the fact that this is different in each case. This is not necessarily true at later times, because the heating distribution depends on the flow evolution. In the absence of rotation one would expect the adiabatic contribution to be negative in the SA case, because the flow must ascend over the heat source. That is true in our case also, but there the ascent is

maximized at the radius of maximum heating which lies off the axis, i.e. one cannot rule out axial subsidence in this case. In the presence of rotation, the adiabatic contribution is larger in the SA case because there is actual subsidence over the heat source; moreover, this is larger than the axial subsidence in our calculation. This can be seen in Fig. 4 which compares the vertical-velocity distribution, $w(R, z)$, at 48 and 120 hours in the SA calculation with that in our own. The calculation of w is described briefly in the appendix. In the early stages of the SA calculation (e.g. at 48 hours), there is upward motion along the entire axis, but by 120 hours, subsiding motion has become established at all heights along the vortex core. In our own calculation, subsidence surrounding the axis occurs also at all heights, but is largest in the lower half of the troposphere. The occurrence of subsidence is in line with the discussion of Smith (1980) and can be explained as follows. Let p denote the perturbation pressure relative to the far environment. If we integrate

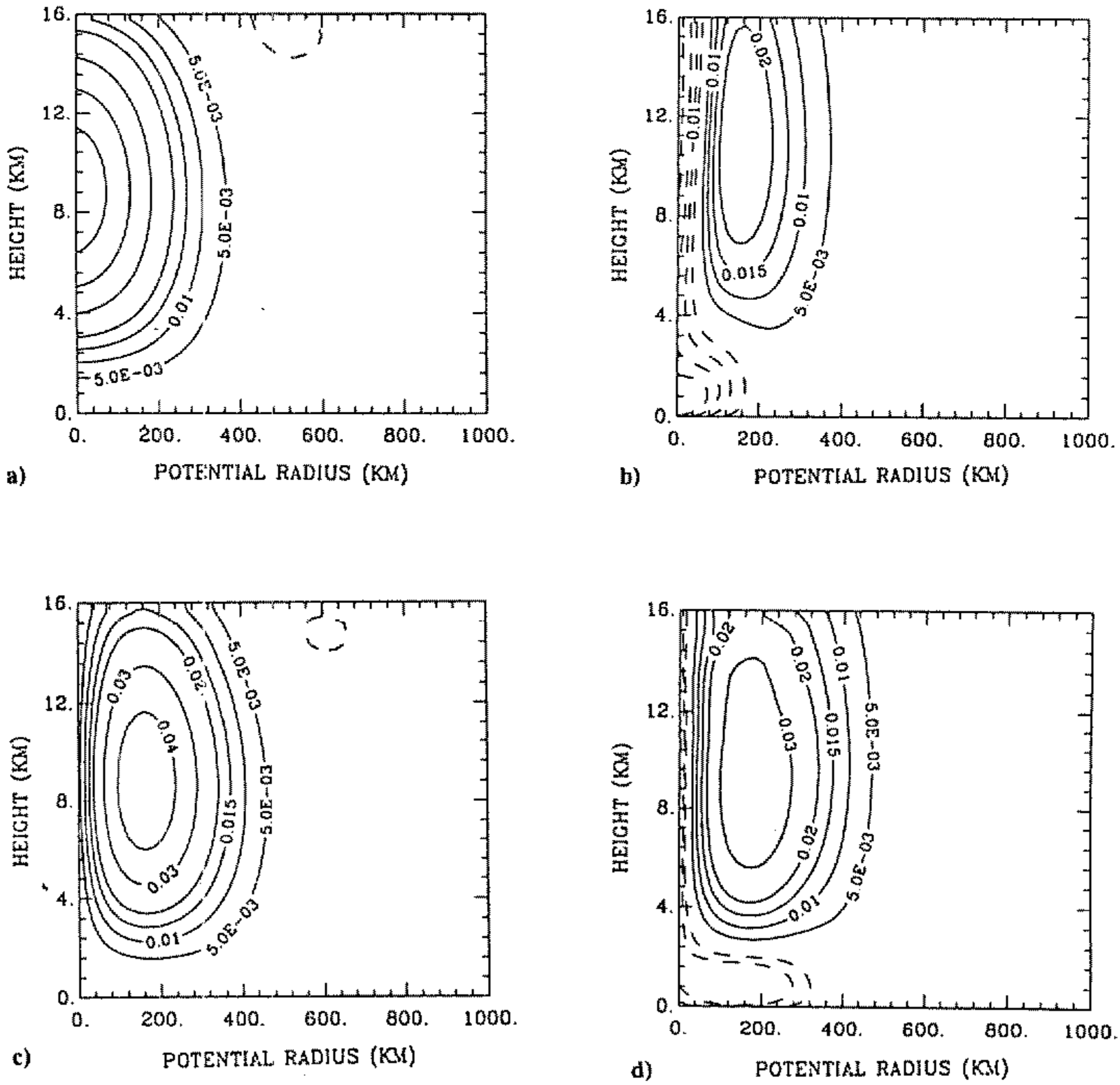

Figure 4. Isolines of the vertical velocity, w, (m s^{-1}) in (R, z) space corresponding with the calculations in Figs. 1 and 2. (a) and (b) are for the Schubert and Alworth heating function at 48 hours and 120 hours, with minima of 0.0028 m s^{-1} and 0.029 m s^{-1}, respectively. (c) and (d) are for the annular heating function at 48 hours and 120 hours, with minima of 0.0026 m s^{-1} and 0.011 m s^{-1}, respectively.

the gradient wind equation $\rho v(v/r + f) = \mathrm{d}p/\mathrm{d}r$ with respect to radius, from the axis $r = 0$ to some large radius, where the perturbation pressure is small, we obtain essentially

$$-p(0, z) = \int_0^\infty \rho\left(\frac{v^2}{r} + f v\right) \mathrm{d}r. \tag{12}$$

Differentiating this equation with respect to height and dividing by the density ρ gives

$$-\frac{1}{\rho}\frac{\partial p}{\partial z} = \frac{1}{\rho}\frac{\partial}{\partial z}\int_0^\infty \rho\left(\frac{v^2}{r} + f v\right) \mathrm{d}r. \tag{13}$$

In a hurricane, the dominant contribution to the right-hand side of Eq. (13) is from the centrifugal force. Subsidence along the vortex axis requires a downward-acting perturbation pressure gradient. Equation (13) shows that this gradient is associated with a decay and radial spread with height of the tangential-velocity distribution. For SA's heating distribution, the decay of the tangential-velocity distribution with height is stronger than in our calculation and is consistent with stronger subsidence (not shown). Thus the adiabatic contribution to the descent of the isentropes is larger near the vortex axis. The diabatic contribution is also larger, being greatest in the region where the heating is largest.

It is obvious that there are limitations of these fixed heat sources and it would be desirable to implement a more realistic representation of convection in the model and to include friction. Efforts are currently under way to do this.

Acknowledgement

The authors would like to thank Professors Wayne Schubert and Alan Thorpe and two anonymous reviewers for their helpful comments on this work. We gratefully acknowledge support for this work from the German Research Council (DFG) and the US Office of Naval Research through grant No. 00014-90-J-1487.

Appendix

The material derivative of θ in (R, z, t) space can be written as

$$\dot{\theta} = \frac{\mathrm{d}\theta}{\mathrm{d}t} = \left(\frac{\partial\theta}{\partial t}\right)_{R,z} + \dot{R}\left(\frac{\partial\theta}{\partial R}\right)_z + w\left(\frac{\partial\theta}{\partial z}\right)_R.$$

The second term on the right-hand side vanishes because the friction is set to zero (i.e. $\dot{R} = 0$). The calculation of the vertical velocity is obtained from the generalized vertical velocity in the θ system, given by the formula

$$\dot{\theta} = \frac{\mathrm{d}\theta}{\mathrm{d}t} = -\left(\frac{\partial\theta}{\partial z}\right)_R\left(\frac{\partial z}{\partial t}\right)_{R,\theta} + w\left(\frac{\partial\theta}{\partial z}\right)_R$$

which can be rearranged to yield

$$w = \dot{\theta}/\left(\frac{\partial\theta}{\partial z}\right)_R + \left(\frac{\partial z}{\partial t}\right)_{R,\theta}$$

where z is given by Eq. (10).

REFERENCES

Eliassen, A 1952 Slow thermally or frictionally controlled meridional circulation in a circular vortex. *Astrophys. Norv.*, **5,** 19–60

Gray, M. G. and Shea, D. J. 1973 The hurricane's inner core region. II. Thermal stability and dynamic characteristics. *J. Atmos. Sci.*, **30,** 1565–1576

Haynes, P. H. and McIntyre, M. E. 1987 On the evolution of vorticity and potential vorticity in the presence of diabatic heating and frictional or other forces. *J. Atmos. Sci.*, **44,** 828–841

1990 On the conservation and impermeability theorems for potential vorticity. *J. Atmos. Sci.*, **47,** 2021–2031

Hsu, Y. J. G. and Arakawa, A. 1990 Numerical modelling of the atmosphere with an isentropic vertical coordinate. *Mon. Weather. Rev.*, **118,** 1933–1959

Schubert, W. H. and Alworth, B. T. 1987 Evolution of potential vorticity in tropical cyclones. *Q. J. R. Meteorol. Soc.*, **113,** 147–162

Smith, R. K. 1980 Tropical cyclone eye dynamics. *J. Atmos. Sci.*, **37,** 1227–1232

Smith, R. K., Ulrich, W. and Dietachmayer, G. 1990 A numerical study of tropical cyclone motion using a barotropic model. I: The role of vortex asymmetries. *Q. J. R. Meteorol. Soc.*, **116,** 337–362